ChemComm

Accepted Manuscript

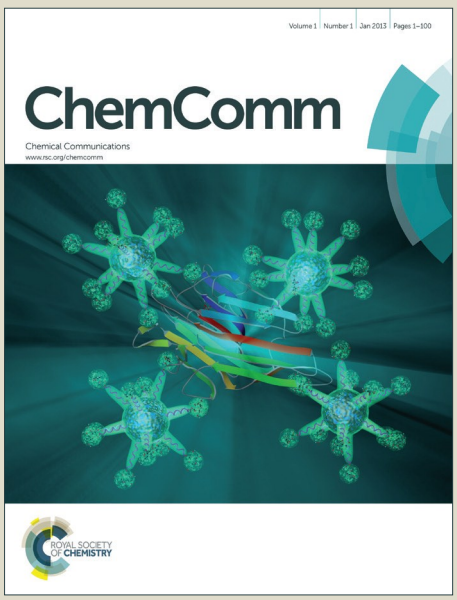

ROYAL SOCIETY OF CHEMISTRY

www.rsc.org/chemcomm

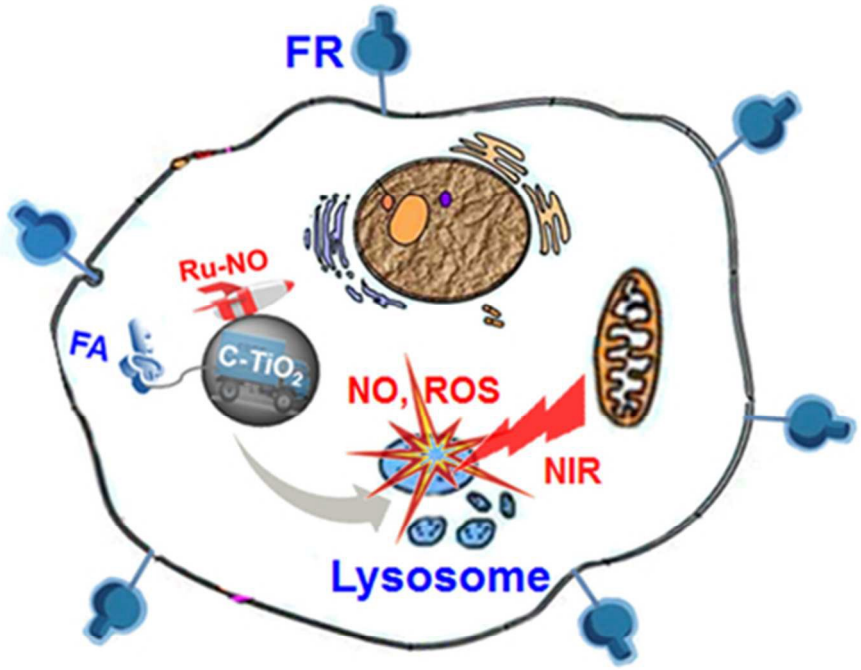

39x32mm (300 x 300 DPI)

Chem. Commun.

RSCPublishing

COMMUNICATION

Tumor Cell Specific and Lysosome-targeted Delivery of Nitric Oxide for Enhanced Photodynamic Therapy Triggered by 808 nm Near-Infrared Light

Cite this: DOI: 10.1039/xoxxoooooox

Received ooth January 2012,
Accepted ooth January 2012

DOI: 10.1039/xoxxoooooox

Hui-Jing Xiang,[†] Qiao Deng,[†] Lu An,[‡] Min Guo,[†] Shi-Ping Yang[‡] and Jin-Gang Liu[†]

A novel cancer cell lysosome-targetable multifunctional NO-delivery nanoplatform (Lyso-Ru-NO@FA@C-TiO_2) (1) was developed. It selectively targets folate-receptor overexpressed cancer cells and specifically locates within the lysosome organelle to which NO and reactive oxygen species are simultaneously released upon 808 nm NIR light irradiation. The dual-targeted nanoplatform (1) demonstrated the highest anticancer efficacy compared with nontargeted counterparts under NIR light sensitization.

Nitric oxide (NO) not only plays critical roles in various physiological processes but also has been implicated in cancer biology.[1] It has been shown to have both tumoricidal and tumor-promoting effects, depending on its timing, location, and concentration.[1] At high concentrations (≥μM), NO acts as a potent anticancer agent, promoting apoptosis and inhibiting angiogenesis. Development of NO-hybrid drug that combines NO to existing drugs such as photosensitizing agents employed in photodynamic therapy (PDT) may afford an advantage of adding the effects of NO to the benefits of drugs to overcome tumor cell resistance to conventional therapeutic agents.

In this context, a wide range of NO donors and their NO-delivery platforms have been developed, among which the light-triggered NO-delivery platforms are particularly attractive. This is the case because light represents a suitable trigger for enabling both spatial and temporal control over NO release.[2-5] However, most of the reported photoreactive NO-delivery platforms have been effective only under UV or visible light irradiation, where excitation wavelengths suffered from the small depth of tissue penetration as well as cell photodamage from short wavelength light. Given its less-damaging and minimal absorbance by skin and tissues that allows for noninvasive deeper penetration, near-infrared (NIR) light is apparently more advantageous as a light trigger for NO delivery,[6a] especially for an 808 nm NIR light that has the minimized water overheating effect compared with other NIR wavelength, e.g. 980 nm.[6b] Only a few limited examples have demonstrated NIR light-triggered NO release.[4, 7]

Lysosomes are important subcellular acidic organelles for cellular homeostasis, and lysosomal dysfunction is responsible for several diseases. Progressive evidence has suggested that the lysosomal death pathway could markedly contribute to the programmed cell death sensitivity of cancer cells.[8] Thus, the development of a NO-hybrid drug that specifically delivers NO to lysosomes will render the drug with maximal therapeutic efficacy and minimal side effects.

Herein, we report a novel cancer cell lysosome-targetable multifunctional NO-delivery nanoplatform (Lyso-Ru-NO@FA@C-TiO_2) (**1**). This nanoplatform selectively targets folate-receptor (FR) overexpressed cancer cells and specifically locates within the lysosome organelle to which NO and reactive oxygen species (ROS) are simultaneously delivered upon 808 nm NIR light irradiation with mild power intensity (200–600 mW/cm^{-2}) (Figure 1).[9] This represents the first example of cancer cell lysosome-specific codelivery of NO and ROS on demand with the controlled NIR light.

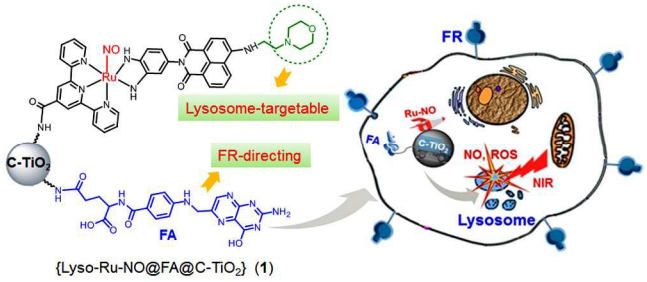

Figure 1. Schematic representation of nanoplatform (1) and the directed-attack of cancer cell lysosomes by NO and ROS under NIR light irradiation.

The NO-delivery nanoplatform (**1**) is composed of a ruthenium nitrosyl donor, $[Ru(tpy^{COOH})(Lyso\text{-}NINO)(NO)]$ $(PF_6)_3$, (Lyso-Ru-NO), a cancer cell directing group of folic acid (FA), and a carrier of biocompatible carbon-doped titanium dioxide nanoparticles (C-TiO_2 NPs). The designed novel ruthenium nitrosyl Lyso-Ru-NO contains a ligand of Lyso-NINO wherein a morpholine moiety serves as a well-known lysosomal targeting group.[10] The FA group is used as a tumor-targeting component on the basis of its high affinity to FR, which is often overexpressed on the surface of a wide range of human cancerous cells (e.g., HeLa and KB cell lines).[11] Given its unique photocatalytic properties, good biocompatibility, and low cytotoxicity, TiO_2 NPs have been well documented in the biomedical applications of PDT and drug delivery.[12] Carbon doping may generate new hybrid states in the band gap of TiO_2, which renders C-TiO_2 NPs with significant absorbance in long wavelength regions.[13] Thus, we employed C-TiO_2 NPs as carriers for NIR light-triggered NO delivery, expecting that at the same time C-TiO_2 NPs may work as efficient photosensitizers to generate cytotoxic ROS under NIR light illumination.

The procedures for the preparation of the ruthenium nitrosyl Lyso-Ru-NO and its corresponding NO-delivery nanoplatform (**1**) are described in the supporting information. The morphology of nanoplatform (**1**) was examined using transmission electron microscope (TEM), which displayed a spherical morphology with diameters of about 4 nm (Figure 2A). Its surface chemical composition was then analyzed using X-ray photoelectron spectroscopy (XPS). The XP survey spectrum revealed signatures of C, F, N, O, P, Ru, and Ti (Figure 2B). The high resolution N1s XP spectrum of nanoplatform (**1**) showed one broad nitrogen signal that was deconvoluted into several components as indicated in Figure 2C. The N1s peak at 402.0 eV was assignable to the nitrogen atom of nitrosyl.[14] The amount of Lyso-Ru-NO incorporated onto the surface of C-TiO_2 NPs was determined to be 6.64 wt% Ru, which corresponds to 0.65 μmol NO per milligram of the nanoplatform.

The diffuse reflectance UV/vis-NIR absorption spectrum of nanoplatform (**1**) showed significant enhancement of light absorption at wavelengths of 600–1200 nm than C-TiO_2 NPs, suggesting the grafting of Lyso-Ru-NO onto the surface of C-TiO_2 NPs further intensified its absorbance in the long wavelength region (Figure 2D). The FTIR spectrum of nanoplatform (**1**) displayed a ν_{NO} peak at 1891 cm^{-1} (Figure 2D inset), which slightly shifted to higher energy than that of uncoupled ruthenium nitrosyl Lyso-Ru-NO (1898 cm^{-1}, Figure S1B, ESI). Nanoplatform (**1**) exhibited a photoluminescence peak centered at 468 nm (Figure S2, ESI) when exited at a wavelength of 280 nm. This blue fluorescence characteristic makes it possible to track the nanoplatform in cells. The X-ray diffractive (XRD) spectra of nanoplatform (**1**) displayed patterns similar to those of C-TiO_2 NPs with (101), (004), (200), and (105) reflections that are characteristics of anatase TiO_2 (Figure S3, ESI). This result indicates that the surface incorporation of ruthenium nitrosyl does not alter the C-TiO_2 NPs structure.

NIR light-triggered NO release from nanoplatform (**1**) was probed using an ultrasensitive NO electrode, which directly detects NO using an amperometric technique. As shown in Figure 3A, incremental NO flux was obtained when the suspension saline solution of nanoplatform (**1**) was irradiated by an 808 nm NIR laser with duration time increasing from 10 s to 40 s under very mild power intensity (200 mW/cm^2).[9] The delivered NO flux was readily tuned by laser pulse through varying both the pulse duration time and pulse intensity (Figure S4A, B, ESI). Moreover, the off-and-on behavior of NO release from nanoplatform (**1**) revealed constant "zig-zag" release profiles (Figure 3B), which indicated a fast response of nanoplatform (**1**) to the applied NIR laser and also suggested that nanoplatform (**1**) has no light fatigue effect under repeated off-and-on laser irradiation. A 1.0 mg/mL of the nanoplatform (**1**) sample suspended in a saline solution can produce a steady level of NO with concentrations more than micromolar (≥ μM) under constant 808 nm NIR light illumination even with light intensities as lower as 200 mW/cm^2 (Figure 3C). Therefore, these results unambiguously demonstrate that efficient NO release from nanoplatform (**1**) can be achieved under the total control of an 808 nm NIR laser while with mild power intensity. The quantum yield (Φ_{NO}) for NO release from nanoplatform (**1**) under 808 nm light irradiation was measured to be 0.0174 ± 0.002 mol $Einstein^{-1}$. In addition, nanoplatform (**1**) showed good stability under various conditions when kept in the dark, even under acidic solutions (Figure S5, ESI). Photo-triggered electron transfer and energy transfer from the C-TiO_2 to the NO donor and the surrounding O_2 are supposed to be responsible for the NO release and ROS generation from the nanoplatform (**1**) under 808-nm laser irradiation (Figure S6, ESI).

The generation of extracellular ROS was then verified using the ROS fluorescent probe 2,7-dichlorofuorescin diacetate (DCFH DA).[15] The fluorescent intensity of the solution of DCFH DA steadily increased in the presence of nanoplatform (**1**) under 808 nm NIR light irradiation (Figure 3D), which reached an 8.7-fold increase relative to that in the absence of light irradiation. The singlet oxygen quantum yields (Φ_Δ) under 808 nm light irradiation were determined to be 0.23–0.28 with pH from 8.0 to 4.0 (ESI). It is noteworthy that under similar experimental conditions, the fluorescence intensity increased only 2.1 fold for the solution of DCFH DA treated with C-TiO_2 NPs under 808 nm NIR light irradiation (Figure S4C, ESI). These results implicated that nanoplatform (**1**) is more efficient than C-TiO_2 NPs in generating ROS when sensitized by NIR light.

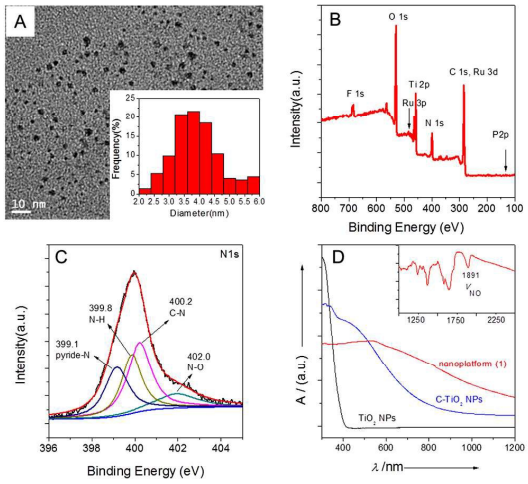

Figure 2. (A) TEM image of nanoplatform (**1**). Inset shows its statistical size distribution. XPS survey (B), and N1s high resolution scan spectra (C) of nanoplatform (**1**). (D) Diffuse reflectance UV/vis-NIR spectra of nanoplatform (**1**) (red line), C-TiO_2 NPs (blue line), and TiO_2 NPs (black line). Inset shows FTIR spectrum of nanoplatform (**1**).

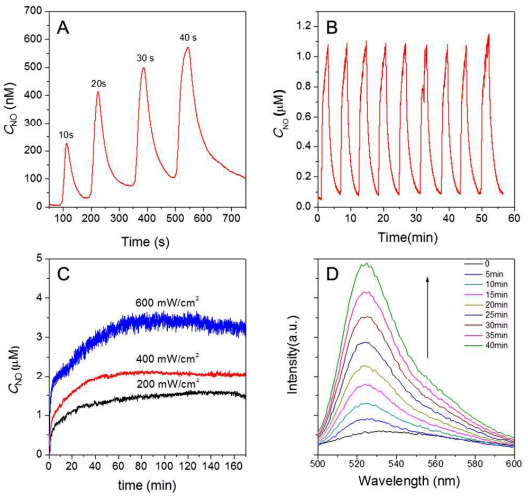

Figure 3. (A) NO flux released from 1.0 mg/mL nanoplatform (**1**) in anaerobic saline solution upon illumination with 808 nm NIR laser pulse (200 mW/cm^2). (B) NIR light-induced NO release from 1.0 mg/mL nanoplatform (**1**) suspended in aerobic saline solution by periodic 808 nm light illumination (600 mW/cm^2). (C) Light-induced NO release from 1.0 mg/mL nanoplatform (**1**) suspended in anaerobic saline solution by constant 808 nm NIR laser illumination with varied light intensitiy. (D) Fluorescence intensity changes of DCFH DA (10 μM) solution in the presence of 1.0 mg/mL nanoplatform (**1**) irradiated by 808 nm NIR light (200 mW/cm^2).

To gain more insight into the nanoplatform (**1**) interaction with cells, we investigated whether or not the FA moiety guides the nanoplatform preferentially to FR-positive tumor cells. FR-positive HeLa cells and FR-negative MCF-7 cells were then incubated with nanoplatform (**1**), respectively. As shown in Figure 4A, the HeLa

cells exhibited strong fluorescence within 2 h of incubation with nanoplatform (**1**), whereas the MCF-7 cells showed very weak fluorescence under the same experimental conditions, (Figure 4B), suggesting the selective accumulation of nanoplatform (**1**) in FR-positive cancer cells. Similar results were obtained using flow cytometry (FCM) analysis. HeLa cells treated with nanoplatform (**1**) yielded far more intense fluorescence compared with MCF-7 cells (Figures 4C and 4D). In addition, competition experiments with free FA were carried out, wherein nanoplatform (**1**) (50 μg/mL) and free FA (50 μg/mL) were incubated together with HeLa cells for 2 h. The result from FCM analysis revealed markedly decreased fluorescence intensity (Figure 4C). As a result, it can be concluded that nanoplatform (**1**) entering into cells was guided by the interactions of its FA moiety with FR on the surface of tumor cells, possibly via receptor-mediated endocytosis.

To further explore the intracellular localization, HeLa cells were treated with nanoplatform (**1**) together with Lysotracker Red, a commercial lysosome tracker. The intracellular localization of nanoplatform (**1**) and Lysotracker Red can then be visualized using confocal laser fluorescence microscopy under different FL channels. Nanoplatform (**1**) is readily visualized by itself in blue fluorescence, and Lysotracker Red is visualized in red fluorescence. The merged image shows the colour of magenta (Figure 5 A) with high Pearson's co-localization coefficient (0.84). This result clearly indicates the internalized nanoplatform (**1**) specifically located in the lysosome organelle. A control experiment with another nanoplatform (Ru-NO@FA@C-TiO_2) was carried out, where the ruthenium nitrosyl was devoid of the lysosome-targeting morpholine moiety. As shown in Figure 5B, the nanoplatform (Ru-NO@FA@C-TiO_2) is randomly distributed inside the cells with Pearson's co-localization coefficient of -0.06, suggesting no specific lysosomal localization. These observations evidently signify the important role of the morpholine group in nanoplatform (**1**) that rendered it to specifically target lysosomes.

The *in vitro* generation of NO was then examined using NO-sensitive fluorescent probe 4-amino-5-methylamino-2′,7′-difluorofluorescein diacetate (DAF-FM DA.[16] HeLa cells were incubated with nanoplatform (**1**) (50 μg/mL) for 4 h and then treated with the DAF-FM DA probe for 30 min. In the absence of light irradiation, only very weak green fluorescence from the probe itself was observed, whereas bright green fluorescence was noticed once the 808 nm NIR laser was applied (Figure S7, ESI), indicating quick NO release from nanoplatform (**1**) within the cells.

Intracellular ROS generation was monitored via the ROS fluorescent probe DCFH-DA. After incubation with nanoplatform (**1**) in the dark, HeLa cells were irradiated with an 808 nm laser. The intracellular fluorescence intensity, as analyzed by FCM, is generally proportional to the amounts of generated ROS. The fluorescence intensity steadily rose with the time of NIR light illumination (Figure S8, ESI), suggesting nanoplatform (**1**) can serve *in vitro* as an efficient photosensitizer under NIR light irradiation for photodynamic therapy.

Subsequently, an MTT assay was performed to evaluate the anticancer efficiency of nanoplatform (**1**) under NIR light irradiation. When treated with nanoplatform (**1**) in various concentrations (10–200 μg/mL) in the dark, the cell viability of both HaLa and MCF-7 cells remained above 85%, suggesting good biocompatibility of the nanoplatform (Figures S9 and S10, ESI). While under the irradiation of an 808 nm NIR laser (600 mW/cm^2, 10 min), the HeLa cell viability remarkably decreased, which showed drug-dosage dependence (Figure 6A). The half maximal inhibitory concentration (IC50) of nanoplatform (**1**) toward HeLa cells under 808 nm NIR light sensitization was about 20 μg/mL. It is interesting to note that the cell viability of FR-negative MCF-7 cells was much higher than that of FR-positive HeLa cells under similar experimental conditions (Figure 7B). In addition, the cell viability was also higher when it was treated with a control nanoplatform (Lyso-Ru-NO@C-TiO_2) without an FA group (Figure 6C). These results implicate the beneficial anticancer effect of the FA-directing group that accounts for more nanoplatform (**1**) accumulation in the targeted cancer cells.

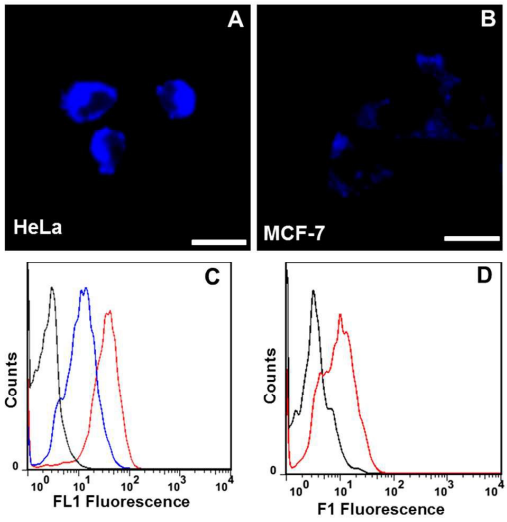

Figure 4. Confocal microscopy images of HeLa (A) and MCF-7 (B) cells treated with nanoplatform (**1**) (50 μg/mL) for 2 h. Excited at 405 nm and detected at 420-490 nm (scale bars: 20 μm). (C) Flow cytometry analysis of HeLa cells treated with 50 μg/mL of nanoplatform (**1**) (red line), 50 μg/mL of nanoplatform (**1**) + 50 μg/mL of FA (blue line) for 2 h. (D) Flow cytometry analysis of MCF-7 cells treated with 50 μg/mL nanoplatform (**1**) for 2 h (red line). The untreated cells were taken as the control (black line).

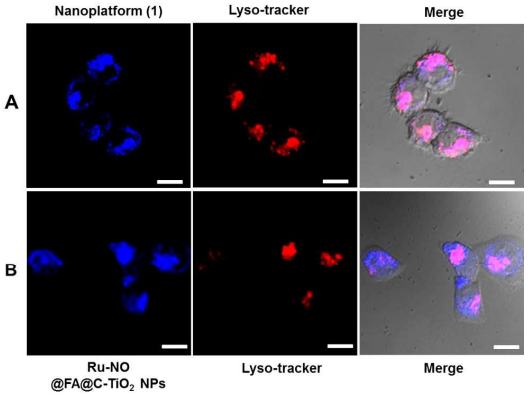

Figure 5. (A) Confocal microscopy images of HeLa cells treated with nanoplatform (**1**) and costained with Lysotracker Red (0.5 μM) for 8 h. (B) Confocal microscopy images of HeLa cells treated with control nanoplatform (Ru-NO@FA@C-TiO_2 NPs) and costained with Lysotracker Red (0.5 μM) for 8 h. The images were acquired for excitation at 405 and 543 nm and recording the corresponding fluorescence in the range of 420–490 nm and 570–620 nm, respectively. Scale bars: 10 μm.

Furthermore, in the absence of the lysosome-targetable morpholine group, the control nanoplatform (Ru-NO@FA@C-TiO_2)-treated HeLa cells also showed higher viability than nanoplatform (**1**) under 808 nm NIR light irradiation (Figure 6C), suggesting that the increased anticancer efficiency was because of the intracellular lysosome-localization of nanoplatform (**1**). Taken together, these results clearly indicate that the dual-targeted nanoplatform (**1**) demonstrated the most efficient anticancer effect.

To differentiate the therapeutic effect exerted by NO and ROS as observed with nanoplatform (**1**), a further control experiment with a

nanoplatform (Lyso-Ru-Cl@FA@C-TiO_2) without coordinated NO was tested for cytotoxicity. With the dosage of 200 μg/mL of nanoplatforms under NIR light sensitization, the viability of HeLa cells treated with (Lyso-Ru-Cl@FA@C-TiO_2) (~46%) was markedly higher than that of HeLa cells treated with nanoplatform (**1**) (~5%, Figure 6C), thus confirming the synergistic cytotoxicity effects of both released NO and ROS. The main cell death mechanism, as revealed by FCM analysis using Annexin V-FITC/propidium iodide (PI) double-staining assay, was suggested to be early apoptosis (Figure S11, ESI).

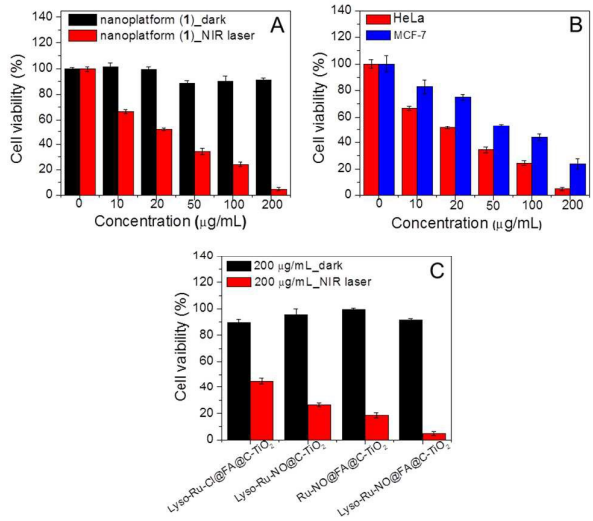

Figure 6 (A) Dark and NIR light-induced (808 nm, 600 mW/cm^2, 10 min) lethality of HeLa cells treated with 0–200 μg/mL nanoplatform (1). (B) Mortality of HeLa and MCF-7 cells treated with nanoplatform (1) under 808 nm laser irradiation (600 mW/cm^2, 10 min). (C) Mortality of HeLa cells treated with 200 μg/mL control samples of (Lyso-Ru-Cl@FA@C-TiO_2 NPs), (Lyso-Ru-NO@C-TiO_2 NPs), (Ru-NO@FA@C-TiO_2 NPs), and the nanoplatform (1) in dark and upon 808 nm laser irradiation (600 mW/cm^2, 10 min).

In summary, a novel multifunctional nanoplatform (**1**), (Lyso-Ru-NO@FA@C-TiO_2), with cellular and subcellular dual-targetable delivery of NO and ROS under 808 nm NIR light irradiation was demonstrated for the first time. The incorporation of FA- and morpholine-directing groups onto the nanoplatform (**1**) renders it capable of targeting FR-positive cancer cell lines and specific accumulations in the subcellular lysosomal organelles. Furthermore, the inherent blue fluorescence of nanoplatform (**1**) enables it to be readily tracked during its cellular internalization and subcellular distribution. The cytotoxicity assay manifested that the dual-targeted nanoplatform (**1**) has the highest anticancer efficacy when compared with the efficacy of nontargeted counterparts under NIR light sensitization. Therefore, this multifunctional platform garnered cancer cell selectivity, subcellular lysosome-targetable, mild NIR light (808 nm, 200–600 mW/cm^2)-triggered NO and ROS release and cell imaging functionalities into one system. Such a novel NO-delivery nanoplatform adds additional NO beneficial effects to traditional PDT and would have new implications for lysosome-targeted and NO-mediated multimodal phototherapy.

This study was financially supported by the NSF of China (21271072, 21571062), the Program for Professor of Special Appointment (Eastern Scholar) at the Shanghai Institutions of Higher Learning, and sponsored by the Shanghai Pujiang Program (13PJ1401900).

Notes and references

[a] *Key Laboratory for Advanced Materials of MOE & Department of Chemistry, East China University of Science and Technology, Shanghai, 200237, P. R. China, E-mail: liujingang@ecust.edu.cn*
[b] *Key Laboratory of Resource Chemistry of MOE & Shanghai Key Laboratory of Rare Earth Functional Materials, Shanghai Normal University, Shanghai, 200234, P. R. China, E-mail: shipingy@shnu.edu.cn*
†Electronic Supplementary Information (ESI) available: Experimental details and additional figures. See DOI: 10.1039/c000000x/

1 A. R. Butler and R. Nicholson, Life, Death and Nitric Oxide, the Royal Society of Chemistry, Cambridge, 2003.
2 (a) M. J. Rose and P. K. Mascharak, *Coord. Chem. Rev*. 2008, **252**, 2093; (b) N. L. Fry and P. K. Mascharak, *Acc. Chem. Res*. 2011, **44**, 289; (c) B. J. Heilman, J. St. John, S. R. J. Oliver, P. K. Mascharak, *J. Am. Chem. Soc*. 2012, **134**, 11573
3 (a) S. Sortino, *J. Mater. Chem*. 2012, **22**, 301; (b) S. Sortino, *Chem. Soc. Rev*. 2010, **39**, 2903; (c) J. Kim, G. Saravanakumar, H. W. Choi, D. Park and W. J. Kim, *J. Mater. Chem. B* 2014, **2**, 341.
4 (a) P. C. Ford, *Nitric Oxide* 2013, **34**, 56; (b) J. V. Garcia, J. Yang, D. Shen, C. Yao, X. Li, R. Wang, G. D. Stucky, D. Zhao, P. C. Ford, F. Zhang, *Small* 2012, **8**, 3800; (c) P. T. Burks, J. V. Garcia, R. GonzalezIrias, J. T. Tillman, M. Niu, A. A. Mikhailovsky, J. Zhang, F. Zhang, P. C. Ford, *J. Am. Chem. Soc*. 2013, **135**, 18145.
5 H. -J. Xiang, L. An, W.-W. Tang, S. -P. Yang, J. -G. Liu, *Chem. Commun*. 2015, **51**, 2555.
6 (a) J. V. Frangioni, *Curr. Opin. Chem. Biol*. **2003**, *7*, 626. (b) X. Xie, X. Liu, *Nat. Mater*. **2012**, *11*, 842.
7 (a) L. Tan, A. Wan, X. Zhu, H. Li, *Chem. Commun*. 2014, **50**, 5725; (b) X. Zhang, G. Tian, W. Yin, L. Wang, X. Zheng, L. Yan, J. Li, H. Su, C. Chen, Z. Gu, Y. Zhao, *Adv. Funct. Mater*. 2015, **25**, 3049.
8 N. Fehrenbacher, M. Jaattela, *Cancer Res*. 2005, **65**, 2993.
9 Using two-photon excitation or upconversion nanoparticles with NIR light to activate the NO-releasing precursors, the excitation power density required was much higher. See references 4 & 7.
10 H. Yu, Y. Xiao, L. Jin, *J. Am. Chem. Soc*. 2012, **134**, 17486.
11 N. Parker, M. J. Turk, E. Westrick, J. D. Lewis, P. S. Low, C. P. Leamon, *Anal. Biochem*. 2005, **338**, 284.
12 (a) Z. Hou, Y. Zhang, K. Deng, Y. Chen, X. Li, X. Deng, Z. Cheng, H. Lian, C. Li, J. Lin, *ACS Nano* 2015, **9**, 2584; (b) C. Ratanatawanate, A. Chyao, K. J. Balkus, Jr., *J. Am. Chem. Soc*. 2011, **133**, 3492.
13 J. Zhong, F. Chen, J. Zhang, *J. Phys. Chem. C* 2010, **114**, 933.
14 K. Artyushkova, B. Kiefer, B. Halevi, A. Knop-Gericke, R. Schlogl, P. Atanassov, *Chem. Commun*. 2013, **49**, 2539.
15 C. Zhu, Q. Yang, L. Liu, F. Lv, S. Li, G. Yang, S. Wang, *Adv. Mater*. 2011, **23**, 4805.
16 H. Kojima, Y. Urano, K. Kikuchi, T. Higuchi, Y. Hirata, T. Nagano *Angew. Chem. Int. Ed*. 1999, **38**, 3209.

